# Stages of spike time variability during neuronal responses to transient inputs

Hugh P. C. Robinson and Annette Harsch
*Department of Physiology, University of Cambridge, Downing Street, Cambridge CB2 3EG, United Kingdom*
(Received 20 May 2002; published 10 December 2002)

In cerebral cortex, cells tend to fire in response to strong transient fluctuations in input, produced by synchronous population activity, which reset the precision of firing and erase correlations between prior and future spike times. Here, using experiments and modeling, we study the accumulation of spike time variance in response to single decaying transient stimuli. All such responses go through distinct stages in time. When the stimulus is high, variance is held low, while at low stimulus levels near threshold, variance rises dramatically, approaching a Poisson level. This behavior was reproduced in a stochastically simulated Hodgkin-Huxley model, and in two simpler models, class 1 (Morris-Lecar) and class 2 (FitzHugh-Nagumo), incorporating Ornstein-Uhlenbeck noise. Early stage variance represents perturbation of uniform limit-cycle motion of the dynamical variables. Late stage variance reflects random motion of the dynamical variables captured within the basin of the resting fixed point. We show that the two stages have different sensitivities to the amplitude and time scale of noise, and relate this to coherence resonance. This rapid breakdown in reliability during responses to transient stimuli may restrict precise signalling by spike times to brief time windows, and limit the duration of coherent synchronous responses in the cortex.

DOI: 10.1103/PhysRevE.66.061902 PACS number(s): 87.19.La, 87.19.Nn, 87.19.Bb

## I. INTRODUCTION

The reliability of spike generation in a neuron depends in a complex way on its input history and on intrinsic noise. There are several important sources of unreliability in spike generation: fluctuations of channel gating [1], of synaptic release [2], or of background presynaptic activity [3]. Experimentally, reliability is measured from responses to repeated presentations of an identical stimulus, often with stationary or periodic properties. Typically, statistics averaged over time, such as response entropy [4], the average jitter of identified repeatable spikes [5] or summed ensemble variance [6] are used to characterize the variability of spike timing.

However, this obscures the time dependence of spike reliability. There is increasing evidence that the activity during physiological responses in the cerebral cortex involves dynamic transients of locally correlated firing in the network [7–9]. Large fluctuations in synchronous network firing can account for the fact that interspike interval (ISI) irregularity in individual cells is far higher than it should be if synaptic input is random and uncorrelated between synapses [10–12]. Strong excitatory input fluctuations play a major role in determining spike timing reliability. The stronger the fluctuation, the more it resets the coherence of the response in an ensemble [5]. With small fluctuations in the input, successive spike intervals remain relatively independent, and the variance in their times of occurrence accumulates. A large excitatory input fluctuation, however, ensures firing within a small window of time, and erases correlation between prior and subsequent spike times. In a complex pattern of input, then, the variability of spike times is repeatedly reset by the larger fluctuations, which can drive bursts of action potentials, of widely varying duration and frequency [13].

Here, we focus on how spike time precision in cortical neurons changes during burst responses to single large input fluctuations, as activity decays from high-frequency firing to silence. We find a blow up in the variance of spike times, which comprises at least two distinct stages. The basis for this is examined in dynamical models of spike generation driven by noisy decaying inputs. The existence of several stages in the blow up of spike time variance is found to be a general property of such models, and can be understood qualitatively by considering the motion of the dynamics in phase space. Finally, we consider possible functional implications of these stages of variability in cortical neuron responses.

## II. VARIANCE OF SPIKE TIMES IN TRANSIENT RESPONSES OF CORTICAL NEURONS

We recorded from layers 2, 3, and 5 pyramidal neurons in slices of rat visual cortex from animals aged 8–27 days, at 33 °C. For details of the preparation, solutions, and whole-cell recording technique, see Ref. [12]. As a stimulus, we used current injection or conductance injection to electrically mimic excitatory synaptic input [14,15]. For conductance injection, each unitary synaptic conductance transient was specified by two phases, representing AMPA and NMDA receptor-mediated components. These components, both reversing at potential zero, were given, respectively, by [in pS, starting from $t=0$ (ms)]

$$g_{AMPA}(t) = 1000(e^{-t/2} - e^{-t/0.5}),$$
$$g_{NMDA}(t) = \frac{62e^{-t/46} + 38e^{-t/235} - 100e^{-t/7}}{1 + 0.6e^{-0.06V}}. \quad (1)$$

### A. Variance during a decaying synaptic conductance

Figure 1 shows the response of a layer *5* cortical pyramidal neuron to repeated stimulation by a burst of unitary excitatory conductance inputs. Unitary inputs are generated by an inhomogeneous Poisson process with an exponentially decaying rate. This stimulus resembles natural stimulation in the sense that, with bursts of this structure injected at stationary Poisson intervals (mean frequency 0.5–2 Hz), the overall

 

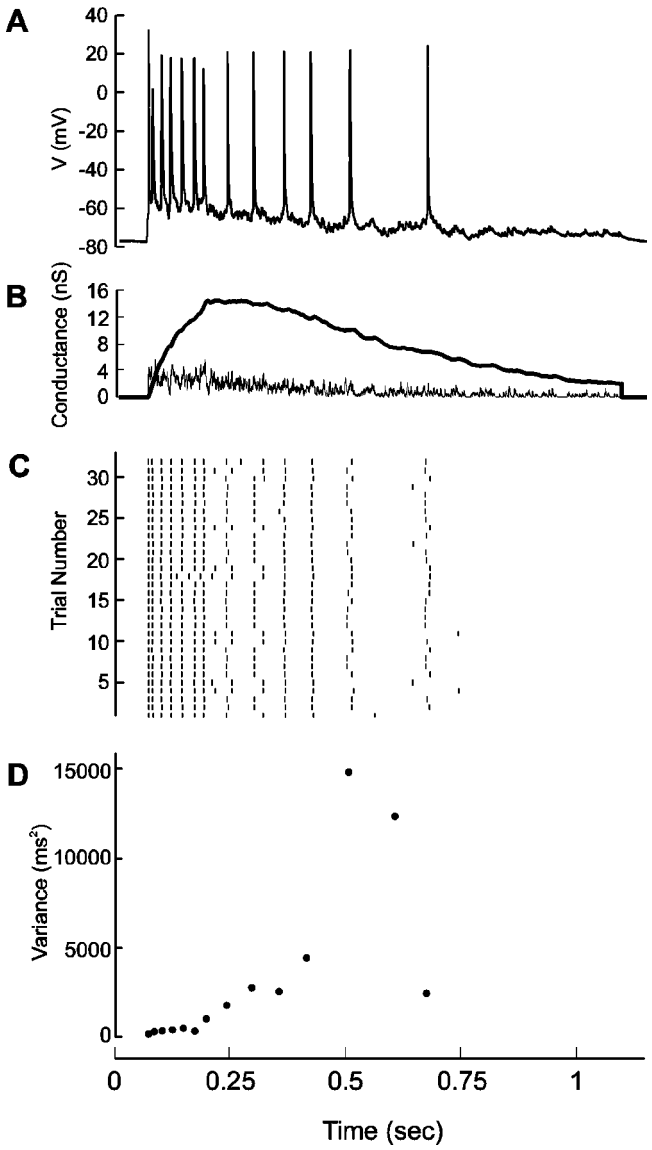


FIG. 1. Spike time variability in response to a layer 5 pyramidal neuron to a natural-like burst conductance input. (a) An example of membrane potential response to a burst conductance input at the soma. (b) Conductance input consisting of a train of unitary AMPA+NMDA conductance transients, generated by a nonstationary Poisson process with an exponentially declining rate. Initial peak rate was 2500 Hz, the time constant of decay of the rate was 500 ms. Total number of unitary input events was 1222. AMPA (thin trace) and NMDA (thick trace) conductance components are shown separately. The NMDA trace shows the commanded conductance; the fraction actually injected is voltage dependent. (c) Raster display of 32 trials with the same stimulus. (d) Variance against mean of successive spike times.

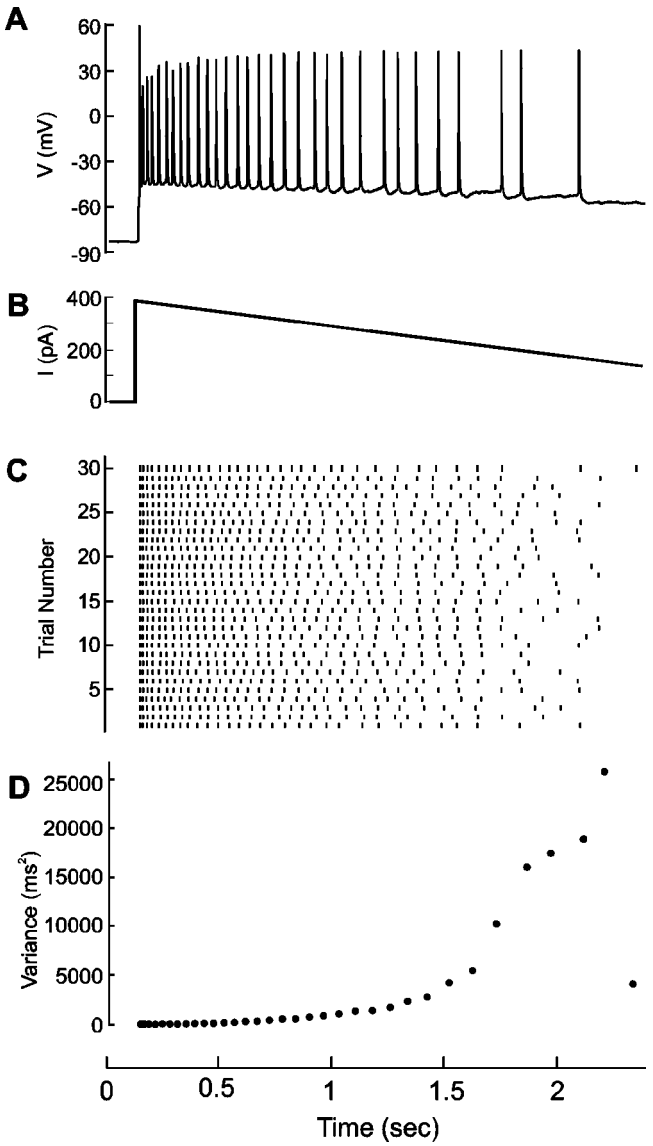


FIG. 2. Variability of cortical neuron spiking responses to decaying ramp current stimuli. (a) A membrane potential response. (b) Current stimulus. (c) Raster display of 30 spike responses. (d) Spike time variance as a function of time.

irregularity of firing as measured by the coefficient of variation of interspike intervals [CV(ISI)] or Fano factor agrees well with *in vivo* levels during spontaneous activity or sensory responses [12], see also Ref. [11]. It is clear from the raster plot in Fig. 1(c) that spike times become markedly less precise with time during the response, owing to intrinsic noise in the spike-generating mechanism of the neuron. In order to quantify this, the variance of spike times in the ensemble is plotted as a function of their mean time of occurrence, in Fig. 1(d).

The variance of spike time $i$ was determined as

$$v_i = \frac{1}{N_i} \sum_{j, n_j \geq i} (t_{ij} - \overline{t_i})^2, \tag{2}$$

where $t_{ij}$ is the time of spike $i$ in response $j$, $N_i$ is the number of responses with $i$ or more spikes, $n_j$ is the total number of spikes in response $j$, and $\overline{t_i}$ is the mean time of spike $i$. If spike intervals have a constant mean and variance and are uncorrelated, then this quantity increases linearly with time.

Several stages are seen in the evolution of the spike time variance. For mean spike times below about 175 ms, variance is very low. It then shows a rapid stage of increase. Finally, for high $i$, variance declines as the number of re-

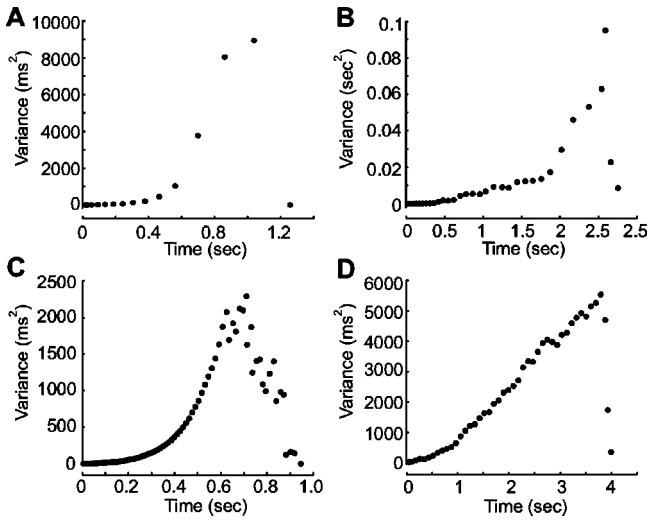


FIG. 3. Spike time variance plots for two types of cortical neuron. (a) A regular-spiking neuron, stimulated by a ramp current decaying from 500 to 0 pA in 3 s. (b) Another regular-spiking neuron, stimulated by a ramp current decaying from 500 to 0 pA in 4.5 s. (c) A fast-spiking neuron, stimulated by a ramp current decaying from 400 to 0 pA in 4 s. (d) A regular-spiking neuron stimulated by a steady current of 100 pA.

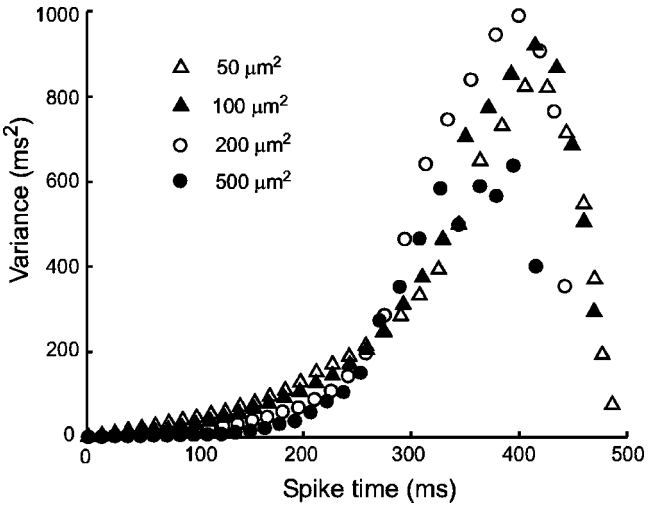


FIG. 4. Spike time variance plots for stochastically simulated Hodgkin-Huxley membrane. Areas of membrane are indicated by a symbol. The stimulus current density decayed linearly from 50 mA/cm$^2$ to 0 over 0–500 ms. Channel density 60 Na channels/$\mu$m$^2$, 18 K channels/$\mu$m$^2$, and capacitance 1 $\mu$F/cm$^2$.

sponses with $i$ or more spikes falls; the times of these spikes are thus constrained by the decline of the stimulus. This basic pattern was observed in all neurons analyzed ($n=7$).

### B. Variance during smooth decaying current ramp

Fast fixed-pattern fluctuations in the decaying conductance stimulus can reintroduce coherence of spiking in the ensemble. To remove this complication, we used a smooth linearly decaying current stimulus (Fig. 2). This showed the same pattern of variance with time, which thus does not depend on the small fluctuations in the stimulus. Other examples of this relationship are shown for regular-spiking pyramidal cells in Figs. 3(a) and 3(b), and for a fast-spiking nonpyramidal cell [Fig. 3(c)]. The same two-stage rise in variance was observed for transient inputs lasting from 0.5–10 s. In contrast, the increase of spike time variance for a steady current stimulus is essentially linear with time [Fig. 3(d)].

## III. SPIKE TIME VARIANCE IN NOISY NEURONAL MODELS

We reproduced qualitatively similar stages of variance in a simple leaky integrate-and-fire (IF) model [25], incorporating a refractory period, when driven by decaying ramps and noise. In the early stage, intervals between spikes are dominated by the constant refractory period, and the variance of intervals is low. In the late stage, the interspike interval becomes determined primarily by the noise in the input, and the variance rises towards the Poisson level. However, in neurons, the characteristics of this phenomenon are expected to depend strongly on the dynamical behavior around the threshold, as well as on the correlation structure of the noise. We, therefore, focussed on more biophysically realistic models of spike generation and noise, both to confirm its existence and to gain further insight into its properties.

### A. Stochastic Hodgkin-Huxley system

We were able to reproduce the two stages of rising variance during decaying input in the stochastic Hodgkin-Huxley model ( [16,17]). In this model, voltage-dependent probabilistic transitions between channel states are simulated explicitly, and the level of voltage noise increases as the area of membrane (and therefore, number of channels) is reduced. At four different membrane areas, the two stages of rising spike time variance are clearly seen in response to the same decaying ramp of current density (Fig. 4). Thus, the stages of spike time variance observed in transient responses of cortical neurons are quite general, appearing in this elementary biophysically based stochastic model of excitability.

An essential difference between the two stages of rising variance is seen: the gradient of the early stage is highly sensitive to the noise level, increasing in inverse proportion to membrane area, while that of the late, high variance stage is almost independent of membrane area. Mean firing frequency decays only slightly during the burst. The point of transition between low and high variance stages is also sensitive to the noise level. The higher the membrane area (i.e., the lower the noise level), the earlier the transition. This leads to a crossover of the relationships at about 270 ms.

### B. The FitzHugh-Nagumo model

We next examine whether this effect arises in even simpler models. We first studied a standard FitzHugh-Nagumo (FHN) model [18] with stationary Ornstein-Uhlenbeck (OU) noise. The two variables, $V$ (activation) and $W$ (inactivation), were given by

$$\dot{V} = V - V^3/3 - W + I(t) + \xi(t), \tag{3}$$

$$\dot{W} = \phi(V + a - bW). \tag{4}$$

The parameters $\phi$, $a$, and $b$ were set to 1/9, 0.7, and 0.8, respectively. The noise term $\xi(t)$ in the derivative of the voltage variable $V$ was updated, for an integration time step of $\delta t$, as follows:

$$\xi(t+\delta t) = \xi(t)\exp(-\delta t/\tau) + n\sigma\sqrt{1-\exp(-2\delta t/\tau)}, \tag{5}$$

where $n$ is a normally distributed random number, $\sigma^2$ is the variance, and $\tau$ is the relaxation time constant of the noise, which is normally distributed in amplitude [19,20]. Euler integration was used, with $\delta t = 0.01$; lower values produced no change in results.

Figure 5(a) shows spike time variance during a decaying ramp stimulus in the noisy FHN system. This shows the same pattern of variance in the response, an initial low rate of increase, followed by a transition to a high rate. In Fig. 5(b), the dependence of early and late stage slopes on $\tau$ and $\sigma$ is shown. $\tau$ was varied over a range of 0.1–10 time units (notionally ms)—about 0.05× to 5× the rise time of the spike, for a constant $\sigma$ of 0.075 input units (notionally A). $\sigma$ was varied over the range 0.04–0.16, at a constant $\tau$ of 1. These values were chosen to represent likely ranges for important sources of physiological noise, relative to spike amplitude and rise time. The early stage slope increased monotonically with $\tau$ and linearly with $\sigma$. The much higher late stage slope, however, was essentially insensitive to $\sigma$ and $\tau$, except at very small values. This corresponds to the above result for the stochastic Hodgkin-Huxley system. For all values of $\tau$ and $\sigma$ used, the coefficient of variation of the interspike intervals was low ($<0.15$) and noise dependent in the early stage, but always attained a value approaching 1 in the late stage, and ISIs approached an exponential distribution (not shown). Thus, in the late stage, the spike train reaches a limit, which resembles a Poisson point process.

The time of transition between early and late stages, from low to high variance, was taken as the time of intersection between the linear fits of the initial early stage and of the late stage. For the FHN system, transition time was increased by a larger amplitude noise: the system is switched to high variance earliest at the smallest noise level. This behavior could be described approximately if the transition occurs when the difference between the mean current level and the noise-free bifurcation level $I_\theta$ is $k-\sigma$, where $k$ is a positive constant. Using a bilinear approximation, the rising phase of the cumulative variance can be described by $\mathrm{Var}(t) = \{m_1 t, t < t_x; m_1 t_x + m_2(t-t_x), t \geqslant t_x\}$, where $m_1$ is the early stage slope, $m_2$ is the late stage slope, and $t_x$ is the transition time. The stimulus current has the form $I(t) = A - at$. At the transition point, $A - at_x = I_\theta + k - \sigma$, so $t_x = (A - I_\theta - k + \sigma)/a$. This accounted for the observed crossover in variance for low and high $\sigma$ (Fig. 6). As $\sigma$ is increased, $m_1$ increases proportionally [Fig. 5(b), top right panel], but $t_x$ is delayed. Although the transition to high variance occurs later for higher noise, the late stage lasts longer. The highest level of variance was actually achieved for an intermediate value of $\sigma$ (0.1).

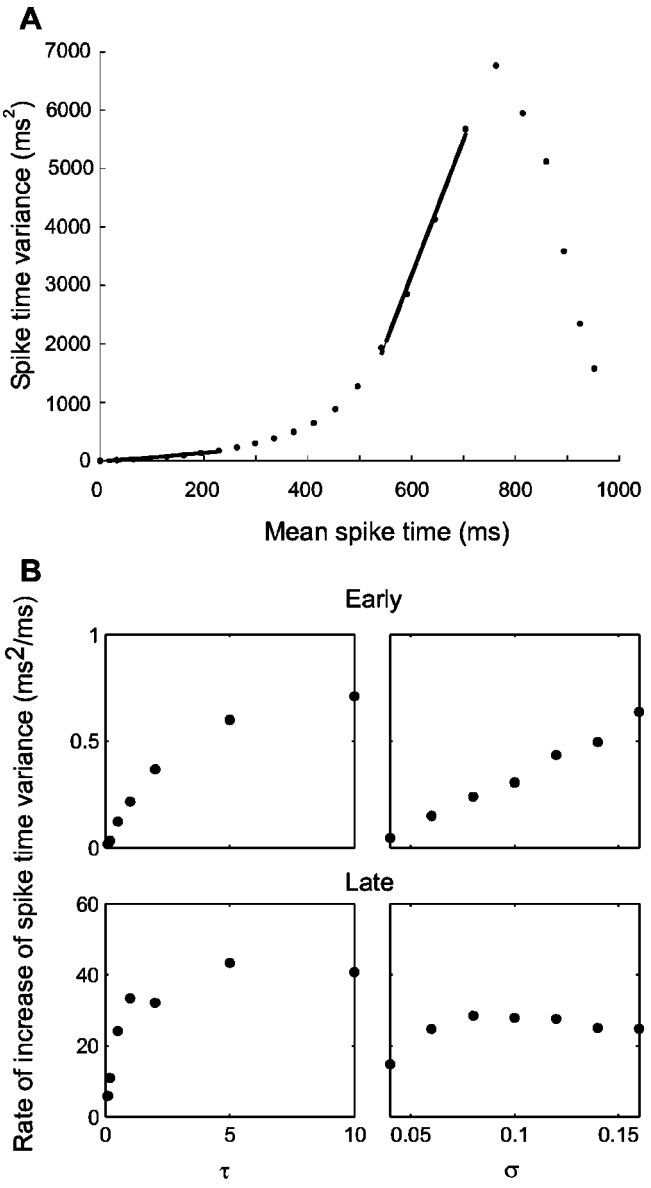


FIG. 5. Spike time variance plot for the noisy FHN model, and sensitivity to the relaxation time and amplitude of noise, for decaying ramp stimuli. (a) Spike time variance as $I$ decays linearly from a value of 0.5 to 0 over 1000 ms. $\sigma = 0.14$, $\tau = 1$. Linear fits to early and late stages of variance growth are shown. (b) Dependence of early and late stage slopes on $\tau$ (at $\sigma = 0.075$) and $\sigma$ (at $\tau = 1$).

### C. The Morris-Lecar type-1 model

Physiological excitable membranes show two basic classes of threshold bifurcation as current stimulus level is increased. In one type, called class 2 [21], there is a sudden transition from rest to a high firing frequency; low-frequency repetitive firing is not supported. This behavior is seen in squid giant axon and in the FHN model, where it corresponds to a subcritical Hopf bifurcation. In the other type of bifurcation behavior (class 1), the frequency-stimulus curve is continuous, so that regular firing of arbitrarily low frequency can be achieved for stimuli just over bifurcation. This

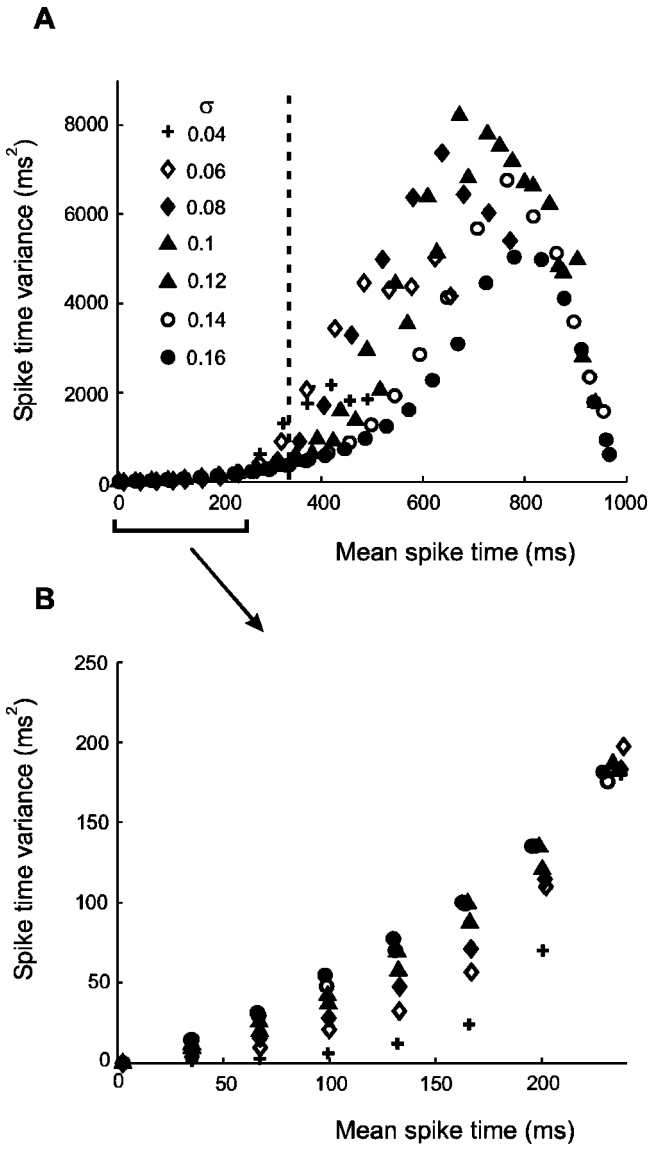


FIG. 6. Sensitivity to noise amplitude ($\sigma$) of spike time variance plots for the noisy FHN model, during decaying ramp stimulation. (a) Spike time variance plots for different values of noise $\sigma$, as $I$ decays linearly from a value of 0.5 to 0 over 1000 time units. $\tau$ was fixed at a value of 1. The time, at which the stimulus ramp decays to the bifurcation point for the noise-free dynamics is indicated by the vertical dashed line. (b) Magnified view of the first stage in (a).

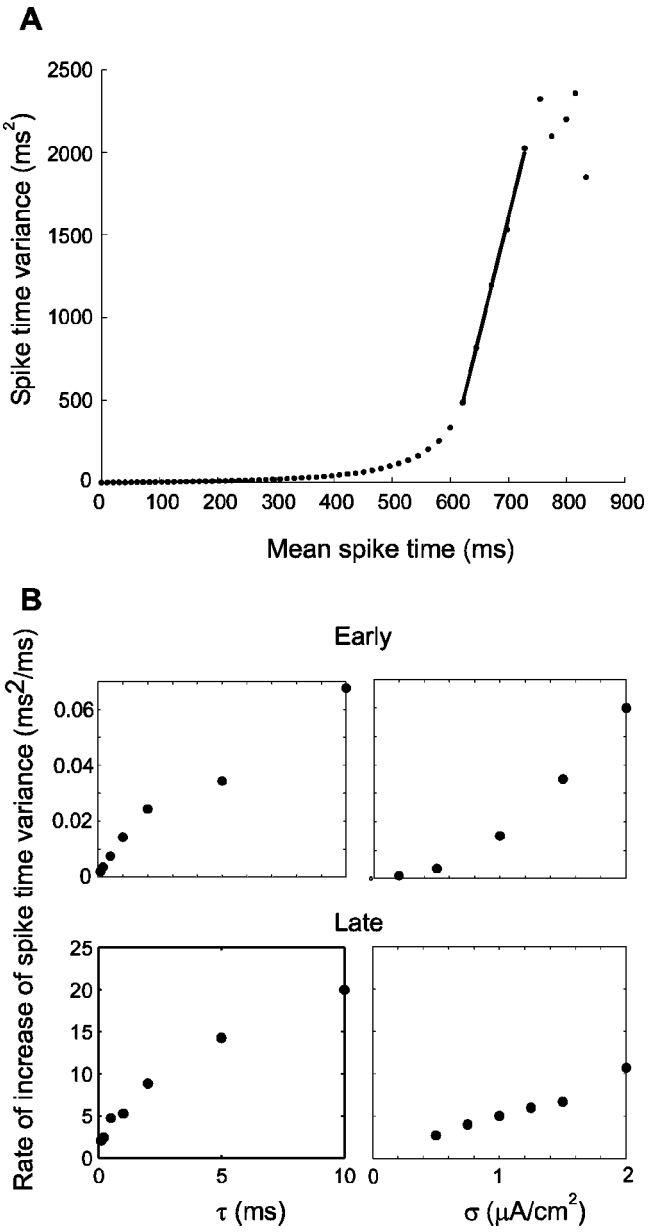


FIG. 7. Spike time variance plot for the noisy ML1 model, and sensitivity to the relaxation time and amplitude of noise, for decaying ramp stimuli. (a) Spike time variance as $I$ decays linearly from a value of 15 to 6 over 1000 ms. $\sigma=5$, $\tau=1$. Linear fits to early and late stages of variance growth are shown. (b) Dependence of early and late stage slopes on $\tau$ (at $\sigma=1$) and $\sigma$ (at $\tau=1$).

behavior is seen in crab nerve, and in the Morris-Lecar equations [22] with class-1 parameters (ML1 model) [23], where the threshold is a saddle-node bifurcation.

The near-bifurcation behavior and sensitivity to noise of a class-1 system may thus have an entirely different pattern from that of a class-2 system [24]. We, therefore, repeated the simulations described above, using the ML1 model (Fig. 7), with a corresponding range of noise parameters. The model is given by

$$\dot{V}=(I(t)+\xi(t)-I_{ionic})/C_m,$$
$$\dot{W}=[W_\infty(V)-W]/\tau_w(V), \tag{6}$$

where

$$I_{ionic}=\overline{G}_{Ca}m_\infty(V)(V-E_{Ca})+\overline{G}_K W(V-E_K)+G_m(V-V_0), \tag{7}$$

$$m_\infty(V)=0.5\left[1+\tanh\frac{V+1}{15}\right], \tag{8}$$

$$W_\infty(V)=0.5\left[1+\tanh\frac{V-10}{14.5}\right], \tag{9}$$

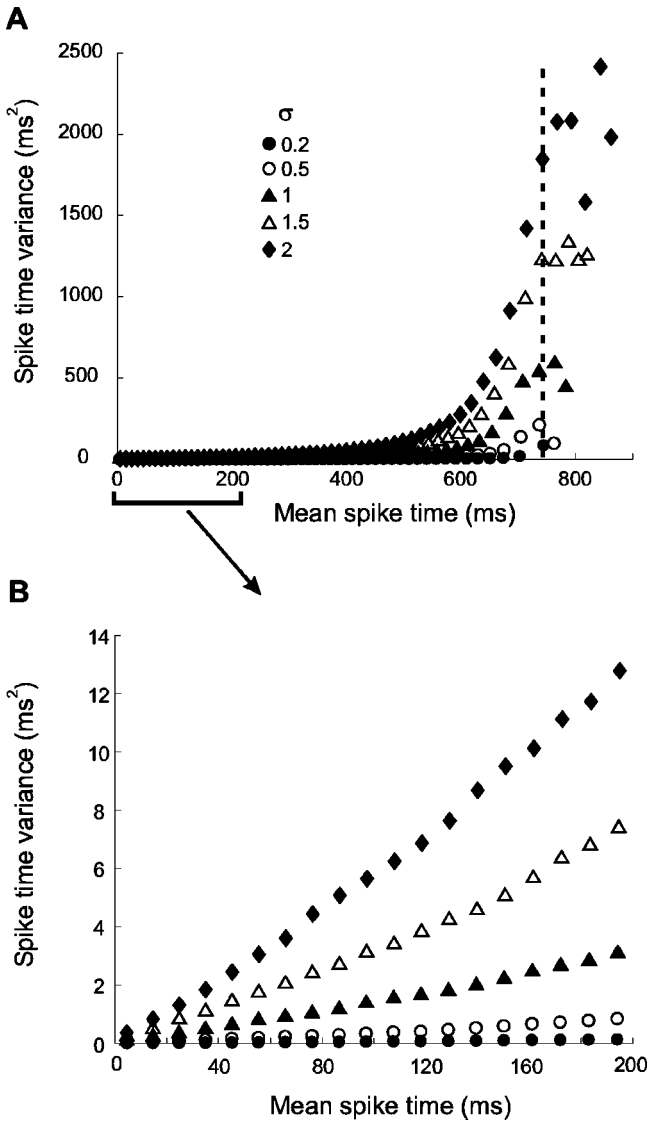


FIG. 8. Sensitivity to noise amplitude ($\sigma$) of spike time variance plots for the noisy ML1 model, during decaying ramp stimulation. (a) Spike time variance plots for different values of noise $\sigma$, as $I$ decays linearly from a value of 15 to 6 over 1000 time units. $\tau$ was fixed at a value of 1. The time, at which the stimulus ramp decays to the bifurcation point for the noise-free dynamics is indicated by the vertical dashed line. (b) Magnified view of the first stage in (a).

$$\tau_w(V) = \frac{3}{\cosh[(V-10)/29]}. \tag{10}$$

$E_{Ca}$ was 100 mV, $\overline{G}_{Ca}$ was 1 mS/cm$^2$, $E_K$ was $-70$ mV, $\overline{G}_K$ was 2 mS/cm$^2$, $V_0$ was $-50$ mV, and $C_m$ was 1 $\mu$F/cm$^2$. Current density is in units of $\mu$A/cm$^2$.

Two clear stages of rising spike time variance again emerge, but their properties differ in several respects (Fig. 8). First, unlike the class-2 FHN and stochastic Hodgkin-Huxley models, both early and late stage slopes increased monotonically with $\tau$ and $\sigma$. Second, increasing $\sigma$ led to an earlier, rather than a later transition to the late stage. $t_x \approx (A - I_\theta - k - \sigma)/a$, and therefore, unlike the class-2 models, there is

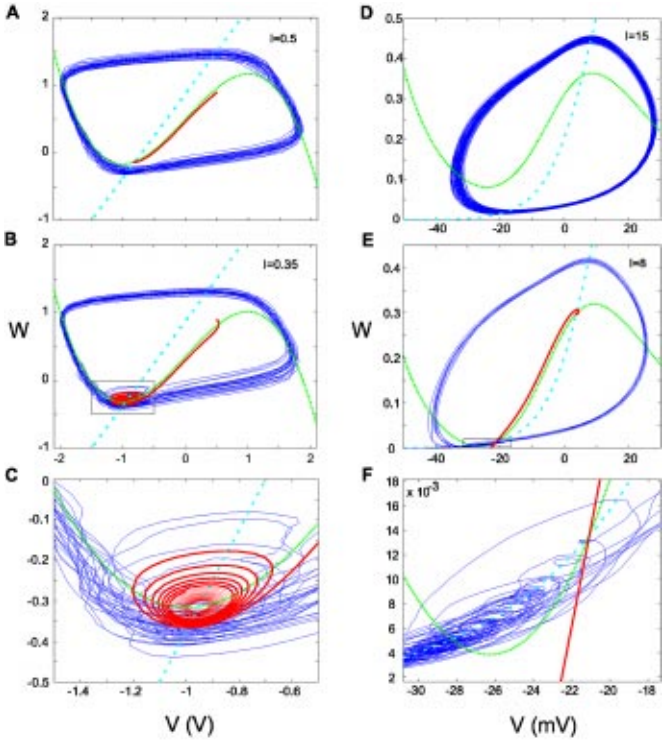


FIG. 9. (Color online) Phase portraits of noisy FHN and ML1 systems at high and near-threshold stimulus levels. Mean stimulus level as indicated in each panel. (a) FHN system, high stimulus level, $I=0.5$. $\sigma=0.075$, $\tau=1$, simulation of 1000 ms. (b) FHN system, stimulus level $I=0.35$ is just above threshold. (c) Enlarged view of the subthreshold region, as indicated by rectangle in (b). (d) ML1 system, high stimulus level, $I=15$. $\sigma=1$, $\tau=2$, simulation of 1000 ms. (e) ML1 system, stimulus level $I=8$ is just below threshold. (f) Enlarged view of the subthreshold region. $V$ nullcline, dotted line; $W$ nullcline, dashed line. Separatrix: thick solid line.

no crossover of variance relationships for different $\sigma$. Like class-2 models, CV(ISI) also increases greatly from early to late stages, but unlike class 2, late stage CV(ISI) also increases steadily with $\sigma$: CV(ISI)$>0.9$ is achieved only for the highest $\sigma$ level used here in Eq. (10).

## IV. BEHAVIOR IN PHASE SPACE

In this section, we visualize the basis for these effects in phase space. Figs. 9(a) and 9(b) show trajectories of the noisy FHN system at two different fixed levels of the stimulus corresponding to early in the decaying ramp and near to the point of transition. $V$ and $W$ nullclines are plotted; their intersection is a fixed point of the dynamics. An effective separatrix for the FHN system (see Ref. [18]) is plotted in Fig. 9(a) by integrating the noise-free equations in reverse time, starting from a point just under the full-blown spike trajectory.

In Fig. 9(a), the stimulus level (0.5) is well above the bifurcation level ($\approx 0.33$), and the system orbits counterclockwise in a perturbed limit cycle. The fixed point and separatrix do not intersect the orbit, and the essential shape of the motion is not changed by the noise. At stimulus levels just above bifurcation, the separatrix starts to intersect the

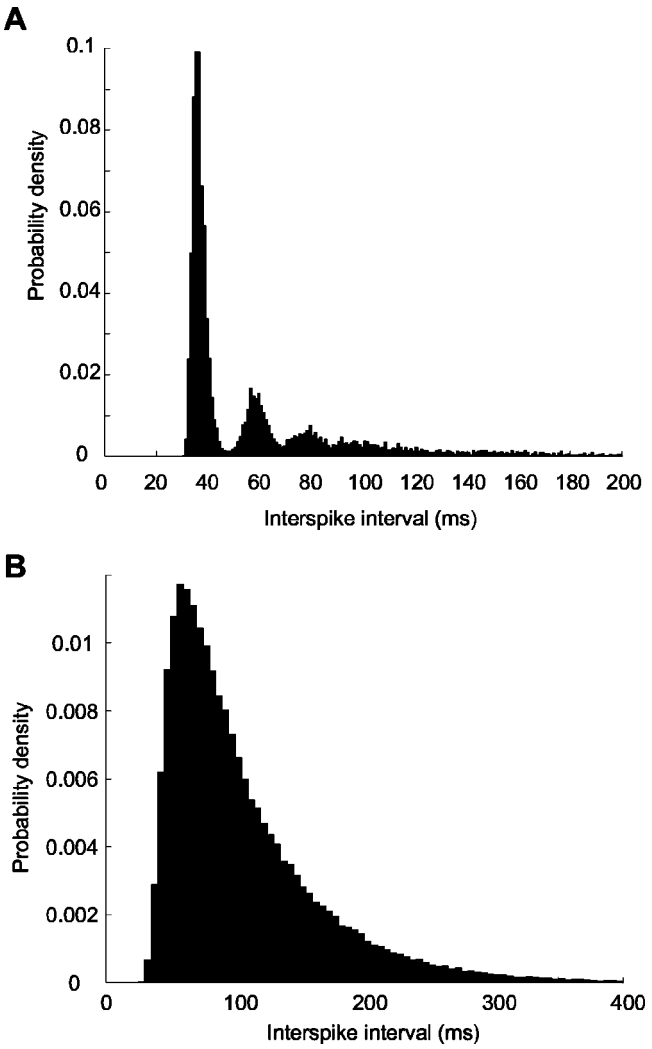


FIG. 10. ISI histograms for noisy FHN and ML1 systems near threshold. (a) FHN system. $\tau=0.1$, $\sigma=0.1$, $I=0.33$. (b) ML1 system. $\tau=1$, $\sigma=0.1$, $I=8.32$

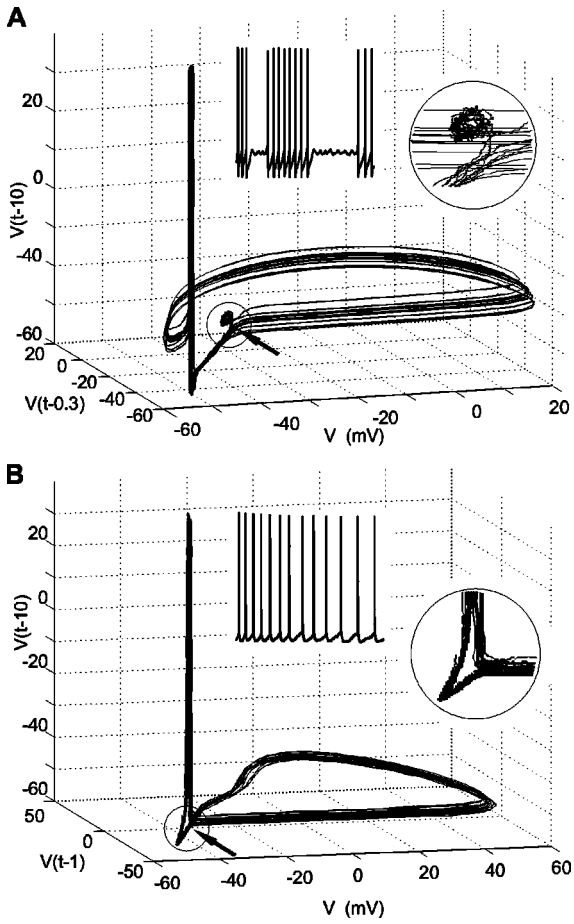


FIG. 11. Time delay reconstruction of phase space in response to cortical neuron near threshold. (a) a fast-spiking neuron stimulated by a constant current of 150 pA. (b) A regular-spiking neuron stimulated by a constant current of 300 pA.

noisy orbit and becomes a dense spiral [Fig. 9(b)]. A small fluctuation can now readily reverse the direction of the trajectory. The phase point is caught for increasing periods in the local basin of the resting fixed point, which becomes intermittently attractive as the stimulus level nears threshold. Small resonant oscillations within this basin are evident at this stage [Fig. 9(c)]. Linearizing the dynamics at the fixed point gives complex eigenvalues [25], so that trajectories starting from small perturbations from the fixed point are oscillatory, with a period of about 20 ms just below threshold. This is in the same range as $\tau$, so that the noise drives subthreshold oscillations effectively. This is reflected in the multimodal ISI distribution [Fig. 10(a)]. At very low stimulus levels, the trajectory mostly executes a random walk in a basin around the fixed point, with essentially a constant probability of escaping to spike at any time, irrespective of history. Consequently, spike generation becomes similar to a Poisson point process, and ISIs become exponentially distributed (not shown).

The threshold of the ML1 system is different. Below threshold, there is a pair of fixed points, one stable and one saddle. The stable manifold of the saddle is a true separatrix. Figure 9(d) shows that at stimuli well above bifurcation, the limit cycle is perturbed uniformly by noise, as for the FHN system. When the mean stimulus level is below bifurcation, the phase point again becomes predominantly stuck in a random walk around the stable fixed point [Figs. 9(e) and 9(f)], again generating much higher spike time variance in the late stage of responses. As already observed, there are detailed differences between noisy FHN and ML1 spike time variance plots (which will be considered further below). However, the basic distinction between early and late stages has a similar explanation for both types of neuron.

In experiments, we observed that regular-spiking (RS) cortical pyramidal neurons show class-1 behavior, supporting stable low-frequency firing, while fast-spiking (FS) inhibitory interneurons switch irregularly between high-frequency firing and silence near threshold (see also Ref. [26]), which is a class-2 behavior. We examined delay reconstructions [27,28] of responses to steady current injection in these two types of cell. Three-dimensional reconstructions are shown in Fig. 11, with lags in the range of 1–10 ms. Trajectories in this space did not reproducibly self-intersect, suggesting that a smooth 1:1 transformation of the motion of the principle underlying dynamical variables was achieved [29]. Using

lags of 1 and 10 ms to unfold movement at fast and slow time scales, FS neurons [Fig. 11(a)] showed two patterns of perturbation—uniform perturbation of the spike loop (horizontal limb) and noisy resonant loops (inset) in a basin, from which there are intermittent escapes to spike. In RS neurons [Fig. 11(b)], uniform perturbation of the spiking loop is seen, but as for the ML1 system, subthreshold movement lacks resonant oscillations (inset). Thus, variability of firing in two major types of cortical neurons, RS and FS, appears to follow the qualitative patterns shown by ML1 and FHN models, respectively.

## V. THE NATURE OF SPIKE TIME VARIABILITY IN EARLY AND LATE STAGES

Here, we discuss further the difference between the early stage (ES) and the late stage (LS). In ES, as shown by Fig. 9, phase trajectories avoid highly sensitive regions of phase space, i.e., the separatrix and the neighborhoods of fixed points, at which the derivative is zero. However in LS, trajectories do hit these sensitive regions. The motion becomes totally dominated by the noise, and the phase trajectory eventually meanders around the fixed point, with occasional escapes to a full-blown spike. This is illustrated in panels (c) and (f) of Fig. 9. At low enough levels of noise, the rate of such escapes can be described by Kramer's formula, i.e., as thermal motion escaping from an energy well [17,30].

Recent insights into the phenomenon of coherence resonance (CR) are relevant. CR can be defined, for example, as the existence of a minimum in CV(ISI) at a nonzero amplitude of noise [31]. It occurs in several models of excitability, including the FHN and Hodgkin-Huxley models when driven by noise. CR arises from different sensitivities to noise in slow and fast motions of the dynamics [32]. Slow motions (i.e., around a fixed point) are highly sensitive, and the CV of periods spent in slow motion rises as noise amplitude is reduced. However, the CV of the periods of fast motion, i.e., spikes, increases with noise amplitude. The progressive shift from slow to fast motion as noise amplitude increases, thus, leads to a minimum in spike interval variability. CR can also be seen as a function of noise $\tau$ [33]. In the responses to transient decaying inputs shown in this study, the ES is mainly fast motion, while the LS is mainly slow motion. During the period of transition, there is a progressive increase in the content of slow motion. In CR, the noise amplitude is the variable, which controls the fast versus slow content of motion. Here, however, noise amplitude is constant, while the switch from fast motion to slow motion is effected by the decaying mean level.

## VI. SPIKE TIME VARIABILITY IN CLASS-1 AND -2 NEURONS

The ML1 model shows a major difference from the FHN model, namely that the gradient of the variance-time plots during LS increases with the noise $\sigma$ or $\tau$ [see Figs. 7(b) and 8(a)], as does CV(ISI). The nature of the slow motion is different between class-1 and -2 dynamics. First, the characteristic time scale of the dynamics within the basin of the resting fixed point is very slow relative to the noise, unlike for the class-2 FHN dynamics. Linearization of the dynamics around the resting fixed point just below threshold shows that the period of oscillations is around 200 ms for the ML1 model, in comparison to 20 ms for the FHN model [40]. The range of noise $\tau$ investigated in this study is comparable to the characteristic time scale of FHN subthreshold dynamics, but much faster than that of ML1 dynamics. The subthreshold motion of the noisy ML1 dynamics is thus more random, and less oscillatory. Second, in the ML1 model, the motion slows greatly during low-frequency limit-cycle firing above bifurcation as the trajectory approaches the region, where $V$ and $W$ nullclines almost touch. This leads to a more extended period of transition between fast and slow motion during decaying responses. When mean current is above the bifurcation level, large negative noise fluctuations can result in capture of the trajectory in slow motion for long periods, so that $t_x$ shortens rather than lengthens as $\sigma$ increases.

Gutkin and Ermentrout [24] measured the CV(ISI) for ML1 dynamics and a different version of ML dynamics with class-2 parameters, when driven by noise (a Poisson train of charge pulses). Over a certain range of stimulus parameters, they found that class-1 dynamics produced a higher CV(ISI). They suggested that class-1 dynamics are intrinsically capable of producing much higher variability, and that this could explain the high CV(ISI) of cortical cell firing observed *in vivo*. They argued that since the class-1 system can fire at arbitrarily low frequencies above threshold, then fluctuations should map a small range of amplitude variations to a larger range of fluctuations in the firing period. But strictly, this argument applies for considering variations in a steady-state stimulus amplitude, above threshold. We have shown here that both the classes of the model generate much larger variability when mean stimulus levels are *below* threshold. Indeed in decaying responses, the class-2 FHN model robustly achieved higher CV(ISI) than the ML1 model, since its LS variability was nearly maximal (Poisson) over a wide range of noise amplitudes. We found that ML2 dynamics produces the same pattern of responses to decaying ramps as the FHN system, with a crossover in the spike time variance relationships for different $\sigma$, and a constant late stage slope. Thus, we do not ascribe the high CV(ISI) observed in the cortex to the class-1 nature of regular-spiking pyramidal neurons, but rather mainly to the transient burst structure of synaptic input due to correlated population firing patterns [12], and to the class-independent rise in spike time variance as each transient response decays.

## VII. CONCLUSIONS

In this paper, we have investigated variability of spike timing during responses to dynamic or transient inputs, in cortical neurons and in biophysically motivated models of spike generation. Previous work has shown that a slowly varying stimulus leads to high variability of spike times, while a fast-changing stimulus yields low variability [5,34]. This occurs even in IF models, where the spread of the ISI histogram is inversely proportional to $dV/dt$ at threshold [35,36], although IF models driven by stochastic input fail to

show effects observed in more biophysically realistic models [37]. In the stochastic Hodgkin-Huxley model, it has been shown that there are two qualitatively different modes of variability, with greatly enhanced variability at low stimulus levels, when there are small numbers of open channels [38]. In this paper, we have shown that such low and high variability modes are separated in time during responses to transiently decaying stimuli. We have qualitatively explained the dynamical basis of this effect, and described how spike variability is affected by the parameters of the noise, and by the class of the spiking dynamics.

In the functioning cortex, large transients of local population activity are observed [3,7–9], leading to transients of synaptic input and burst firing. They are presumably initiated through the positive feedback of excitation through highly recurrent connections, and terminated by adaptation and inactivation in individual neurons and by short-term depression of excitatory synapses. The onset of a strong input fluctuation resets the synchrony of spike timing in a population of neurons receiving the same input. Therefore, it is natural to consider such transient burst responses as distinct units of firing [13]. The large difference in firing precision between ES and LS clearly has important consequences for responses to transient inputs. Reliable signalling with spike times must be confined to the early period of a transient response, as recently demonstrated for visual responses in the cortex [39]. The response then suffers a progressive and finally very rapid, breakdown in precision of firing. To limit the accumulation of spike time variance, the system should not linger in the LS. Where this is important, particular ionic channels may be expressed to produce rapid repolarization at the ends of bursts, for example, the deactivation of persistent Na channels, or the activation of calcium-dependent K channels. However, LS variability may help to stabilize network firing. Precise responses of individual cells mean synchronous firing in the cortical network, for example, is a potentially runaway phenomenon. However, the rising variance in spike times during a transient response could naturally break up synchrony. The different ways, in which spike timing precision decays in RS and FS neurons could give them different roles in terminating periods of coherent firing.

## ACKNOWLEDGMENTS

We thank Jianfeng Feng and John White for helpful discussions and for their comments on the manuscript. This work was supported by grants from the European Commission and the BBSRC.

[1] J.A. White, J.T. Rubinstein, and A.R. Kay, Trends Neurosci. **23**, 131 (2000).
[2] W. Calvin and C. Stevens, J. Neurophysiol. **31**, 574 (1968).
[3] A. Arieli, A. Sterkin, A. Grinvald, and A. Aertsen, Science **273**, 1868 (1996).
[4] F. Rieke, D. Warland, R. de Ruyter van Steveninck, and W. Bialek, *Spikes: Exploring the Neural Code* (MIT Press, Cambridge, MA, 1997).
[5] Z. Mainen and T. Sejnowski, Science **268**, 1503 (1995).
[6] J.D. Hunter, J.G. Milton, P.J. Thomas, and J.D. Cowan, J. Neurophysiol. **80**, 1427 (1998).
[7] T. Bullock, M. McClune, J. Achimowicz, V. Iragui-Madoz, R. Duckrow, and S.S. Spencer, Proc. Natl. Acad. Sci. U.S.A. **92**, 11 568 (1995).
[8] R. Azouz and C. Gray, J. Neurosci. **19**, 2209 (1999).
[9] M. Tsodyks, T. Kenet, A. Grinvald, and A. Arieli, Science **286**, 1943 (1999).
[10] W.R. Softky and C. Koch, J. Neurosci. **13**, 334 (1993).
[11] C.F. Stevens and A.M. Zador, Nat. Neurosci. **1**, 210 (1998).
[12] A. Harsch and H.P.C. Robinson, J. Neurosci. **20**, 6181 (2000).
[13] J.E. Lisman, Trends Neurosci. **20**, 38 (1997).
[14] H. Robinson and N. Kawai, J. Neurosci. Methods **49**, 157 (1993).
[15] H. Robinson, J. Physiol. (London) **518P**, 9 (1999).
[16] E. Skaugen and L. Walloe, Acta Physiol. Scand. **107**, 343 (1979).
[17] C.C. Chow and J.A. White, Biophys. J. **71**, 3013 (1996).
[18] R. FitzHugh, Biophys. J. **1**, 445 (1961).
[19] R.F. Fox, Phys. Rev. A **43**, 2649 (1991).
[20] D.T. Gillespie, Am. J. Phys. **64**, 225 (1996).
[21] A. Hodgkin, J. Physiol. (London) **117**, 500 (1948).
[22] C. Morris and H. Lecar, Biophys. J. **35**, 193 (1981).
[23] J. Rinzel and B. Ermentrout, in *Methods in Neuronal Modelling*, edited by C. Koch and I. Segev (MIT Press, Cambridge, MA, 1998), pp. 251–292.
[24] B.S. Gutkin and G.B. Ermentrout, Neural Comput. **10**, 1047 (1998).
[25] C. Koch, *Biophysics of Computation-Information Processing in Single Neurons* (Oxford University Press, Oxford, 1999).
[26] J.R. Gibson, M. Beierlin, and B.W. Connors, Nature (London) **402**, 75 (1999).
[27] A. Mees, K. Aihara, M. Adachi, K. Judd, T. Ikeguchi, and G. Matsumoto, Phys. Lett. A **169**, 41 (1992).
[28] H. Kantz and T. Schreiber, *Nonlinear Time Series Analysis*, 2nd ed. (Cambridge University Press, Cambridge, 1999).
[29] F. Takens, *Detecting Strange Attractors in Turbulence* (Springer, New York, 1981), Vol. 898.
[30] H. Lecar and R. Nossal, Biophys. J. **11**, 1048 (1971).
[31] A. Pikovsky and J. Kurths, Phys. Rev. Lett. **78**, 775 (1997).
[32] J.R. Pradines, G.V. Osipov, and J.J. Collins, Phys. Rev. E **60**, 6407 (1999).
[33] J. Casado, Phys. Lett. A **235**, 489 (1997).
[34] L. Nowak, M. Sanchez-Vives, and D. McCormick, Cereb. Cortex **7**, 487 (1997).
[35] R.B. Stein, Biophys. J. **7**, 37 (1967).
[36] J. Feng and D. Brown, Biol. Cybern. **80**, 291 (1999).
[37] D. Brown, J. Feng, and S. Feerick, Phys. Rev. Lett. **82**, 4731 (1999).
[38] E. Schneidman, B. Freedman, and I. Segev, Neural Comput. **10**, 1679 (1998).
[39] J.R. Muller, A.B. Metha, J. Krauskopf, and P. Lennie, J. Neurosci. **21**, 6978 (2001).
[40] H. Robinson and M. Kusano (unpublished).